Analyzing a Non-Sinusoidal Response from a Real-World Solar PV

Chetan Mishra, *Member, IEEE*, Luigi Vanfretti, *Senior Member, IEEE*,
Jaime Delaree Jr. and Kevin D. Jones, *Member, IEEE*

***Abstract*—This letter presents an analysis of a non-sinusoidal response from a transmission-level photovoltaic (PV) solar power plant triggered by a local line outage in Dominion Energy's power system. The uniqueness of this response resides in the fact that its critical component is non-sinusoidal, and unlike typical scenarios, it does not stem from conventional nonlinear power system dynamics. It is also demonstrated how careful and systematic analysis of synchrophasor measurements in the plant, through time-series analysis techniques, can help illuminate the underlying mechanism leading to the atypical response observed.**

***Index Terms*—ambient data, control interactions, inverter-based resources, synchrophasors**

I. Introduction

THE increasing penetration of inverter-based resources (IBR) has resulted in unprecedented dynamic performance [1] challenges. These mostly stem from the fact that both IBR plant and inverter controllers are set with fixed parameters that are not updated regularly to adapt to grid operating conditions that may lead to unforeseen interactions with the grid, both in the case of PV [2] and wind [3], which usually come to surface during outage seasons [1]. Furthermore, the fact that most utilities lack transparent plant models for solar facilities makes it difficult to assess and predict these issues, leaving them with measurements as their only recourse for analysis. In this regard, spectral analysis techniques [4], [5] have greatly enabled data driven continuous monitoring of power system dynamics due to the fact that power systems operate most of the time under normal conditions and may therefore be well approximated by linear models estimated solely from measurement data. These techniques analyze measurements in the frequency domain, where power system dynamics are distinguishable, and furthermore separable with the help of filtering, to enable targeted analysis of the phenomena of interest. In the present work, we exploit these approaches to analyze the root cause behind an atypical solar PV response.

II. Overview

A. Subsystem Under Analysis

The study subsystem consists primarily of 115 kV substations as depicted in Fig. 1, along with pre-event line flows obtained from measurements in per unit. The source of the atypical response to be analyzed is substation C, which is a 74.9 MW ±25 MVAR transmission solar plant. The MW PID control tracks a manual set point, curtailed by expected maximum output (based on irradiance) and a ramp rate limit of 8 MW/min. Regarding the VAR control, the plant can operate in PF, Q or AVR mode with Q limits set based on ± 0.95 PF and a ramp rate limit to ensure smooth transition between those modes. It is connected to the rest of Dominion Energy's power system through substations B and A. The shortest electrical path from C to the 230 kV network is through Substation B, which is directly connected by a short line to a 115/230 kV substation. The closest conventional generating unit is a 95 MW hydro plant that is connected through Substation A. In Fig. 1, 115 kV lines are colored red while 230 kV lines are blue. Synchrophasor measurements (i.e., PMU data) are available from the digital fault recorders (DFR) at Substation C on the high side of the PV plant, Lines C-A and C-B, and at Substation A. The DFR specifications are as follows: sampling rate of point on wave data is 4800 Hz, which is filtered and down sampled to 960 Hz from which 60 Hz phasors are estimated. These phasors are then down sampled to 30 Hz and reported.

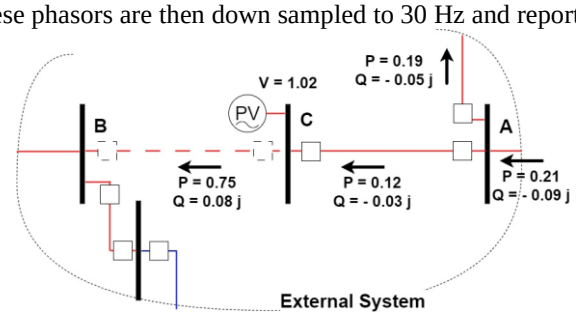

Figure 1. Study Subsystem Single Line Diagram.

B. Non-Sinusoidal PV Response Event

In Feb 2021, Line C-B was taken out of service during a planned maintenance outage around 16:01:56, which resulted in a slow, sustained, and square-like response in the voltage magnitude of about ± 3% from the nominal voltage at C as shown in Fig. 2 (in red). This response lasted for about 100s during which the operator had decided to take the solar plant offline but did not. Luckily, as soon as line C-B was connected back to service (around 16:03:21), the atypical response vanished. In Fig. 2, the outage period is shaded light gray. The plant's MW output was also manually reduced during this period, perhaps to mitigate the issue, and then restored.

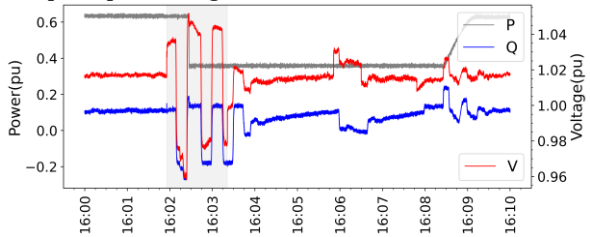

Figure 2. Substation C Solar Response During an Outage.

III. Analysis Results

A. Characterization of Dynamic Behavior

In general, it is common to find several dynamic phenomena in addition to those of interest in real-world power system measurements. Therefore, to narrow down the scope of the analysis, it is necessary to determine the timescale interest. To this end, first, a time-frequency plot of Q output of solar (see Fig. 3) for the time period in Fig. 2 using the continuous wavelet transform (CWT) [6]. Note that unlike short term Fourier transform (STFT), in the CWT the wavelet basis elements usually correspond to a frequency band, which could be wide, to balance time-frequency resolution. Therefore, the y-axis represents the center frequency of the corresponding frequency band and not necessarily the conventional frequency bandwidth. Here, one can see a relatively high signal power in 0.03-0.05 Hz under pre-event and post event ambient conditions, where the previously introduced atypical response of the plant is in the same frequency band, though at a slightly lower frequency, hinting towards a relationship. The reason behind this is that the spectral characteristics of ambient data are typically very similar to those of the impulse or step response for stable dynamics. However, the modal characteristics are typically dependent on the conditions of the system. As a result, the response to a major system change (in our case, a line outage) will not always match the pre-event ambient response because the pre and post-event systems are different, as seen here where the event is at the lower end of the frequency band. Here, we do not know the spectral characteristics to expect during the event (line outage) because we don't have ambient dynamics for the line outage period. Fortunately, once the line was restored to service after the event, there were two periods (labeled in the middle of Fig. 3) where the event response of the plant was seen, like the outage event, though not accompanied by drastic system changes, such as a line outage. As we can see, the spectral characteristics of ambient dynamics and these two responses matched, indicating that all these responses were caused by the same underlying phenomenon (observed under ambient conditions).

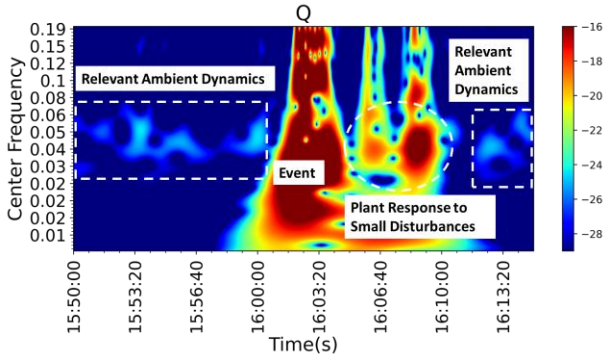

Figure 3. Time-Frequency Representation of the Solar PV's Reactive Power.

Next, we contrast the pre-event (15:55-16:00) and during-event (16:02-16:04) power spectral density estimates [4], as shown in Fig.. 4, to take a closer look at the phenomenon of interest. Observe that both time periods are characterized by not only a dominant frequency in the 0.03-0.05 Hz range (as seen before), but also its odd integer multiples. Furthermore, as seen before in Fig. 3 the event period is marked by a decline in its frequency, from 0.04-0.05 Hz to 0.033 Hz, as shown by a significant increase in the power spectral density (PSD) value. Now, the spectral characteristics of the culprit dynamics present only odd integer multiples of the fundamental frequency, which is typical of square waveform-like characteristic. Expanding the definition of an oscillatory mode to incorporate such behaviors as in [7], these dynamics are referred to as a generalized mode.

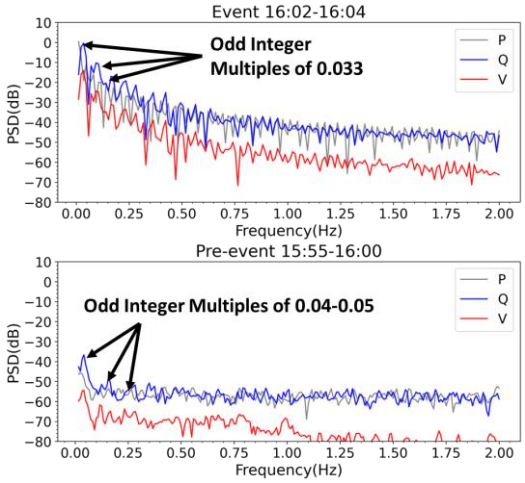

Figure. 4 PSD Estimates.

In addition, note in Fig. 4, that the same mode is only observable in the reactive power output (Q) and voltage magnitude (V) of the plant and not in the active power output (P). This indicates that the unwanted dynamics observed are related to the voltage control system of the PV plant. For P, it simply tracks the maximum power point, which is typical of field installations.

B. Explaining the Non-sinusoidal Response

In this section, we explain the 'square wave'-like characteristics of the mode of interest. These usually occur when non-linearities such as controller saturation are involved, which could be a possible explanation. However, note that the same square-like response persists as the system is stabilizing to equilibrium, and therefore it is unlikely to be large signal-type behavior. Because the phenomenon of interest was identified to be of Q-V type, we narrow our analysis to those signals to understand the underlying mechanism.

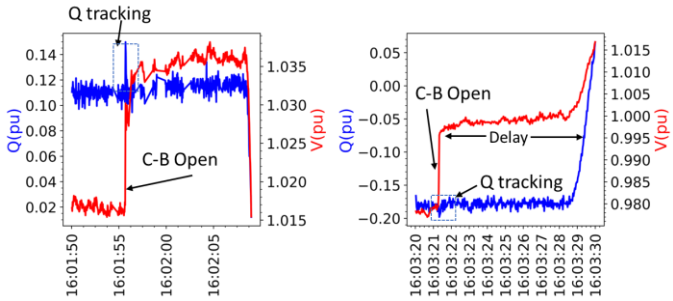

Figure 5. Q and V at Solar during the switching of Line C-B.

First, we analyze the PV plant's response due to the switching of Line C-B at 16:01:53 and 16:03:23 in Fig. 5, which resulted in a step change in the voltage at the solar plant. One can see a momentary jump in Q along with V, with Q quickly

returning to its pre-transient value and staying there for some time. This means that the inverter does not necessarily regulate V but is tracking Q, which is set by the plant controller (referred to from now on as the master controller) and not the inverter itself. This is not surprising since, based on prevailing industry practices [8], there is usually a hierarchical control scheme with the power plant controller operating at slower time scales compared to the internal inverter control loops. Note here that the Q tracking dynamics are fast and well damped, making it difficult here to estimate them accurately [6].

Once the voltage at the solar plant jumps to a new value after switching, a quasi-steady state is momentarily attained for ~10 s after which the master controller changes the Q setpoint to respond to the change in V, which indicates the existence of a large communication delay/lag. Now, only if this holds true for ambient conditions, too, it is possible to assert with certainty that a communication delay exists in the Q-V control loop of the master controller. Unfortunately, the luxury of visual inspection is not available for ambient conditions and given the lack of information about the control scheme in this specific facility, we need to develop a framework to test this hypothesis. Before proceeding, we first preprocess the signals by centering, detrending, applying a low pass filter and down sampling then to a 0-1 Hz range with sampling rate 2 Hz, to retain only the dynamics of interest. Next, we represent the Q-V control loop modeled using an ARX (n_Q, n_V) model structure [9] with output Q and input V owing to the prevalence of linear controllers, particularly PI type used in power systems, the model can be described as,

$$H(z)Q(t) = G(z)V(t) + \epsilon(t) \quad (1)$$

where, $z * x(t) = x(t + \Delta t)$, $\Delta t = 0.5\,s$, $G(z) = \sum_{k=1:n_V} g_k z^{-k}$, $H(z) = 1 - \sum_{k=1:n_Q} h_k z^{-k}$ and $\epsilon(t)$ is Gaussian white noise. Here, an input-output delay of $n_{delay} \times \Delta t$ seconds will result in $g_1 = g_2 \ldots g_{n_{delay}} = 0$, which we aim to infer from the model's response. To do so, we adopt the Granger causality test [10], which uses statistical hypothesis testing to infer whether the future values of a time series (Q) can be estimated by the past values of another time series (V). In this work, it will be done through the following series of F tests on the ARX model in (1),

$$\text{For } n_V = 1{:}\,n_{max} \quad (2)$$
$$H_0{:}\, g_1 = g_2 \ldots g_{n_V} = 0$$
$$H_a{:}\, \exists i \in [1, n_V]\; s.t.\; g_i \neq 0.$$

Fig. 6 shows the F test p values for different values of input n_V lags in seconds ($n_V \times \Delta t$) along with the type 1 error rate $\alpha = 0.05$ threshold (shown by black dotted line) for both pre-event ambient data and during event data. It can be seen in both cases that the delay terms in V of up to 10 s correspond to very high p-values meaning that they can be omitted from the model. However, p-values become significantly low for an 11 s delay, which shows strong evidence in the measurement data to safely reject the null hypothesis in favor of an alternate hypothesis: higher delays in V of 10-12 s are significantly useful in explaining Q. In other words, there is an input-output delay of 10 - 12 s with at least a 95% certainty.

Now, the fundamental frequency of the dominant dynamics was in the 0.03-0.05 Hz range, which corresponds to a time period of 20-33.3 s. In comparison, twice of the 'inferred' controller delay based on the above test is 20-24 s, which is at the lower end of this range. This is not a coincidence, as will be demonstrated through an example simulation. It will also show how the existence of a lengthy delay can cause a response that resembles a square wave. Note that this is only a proof of concept and in no way an attempt to reconstruct the oscillation event precisely via simulation, which is difficult to accomplish in practice due to a lack of adequate models for the PV plant and the rest of the grid.

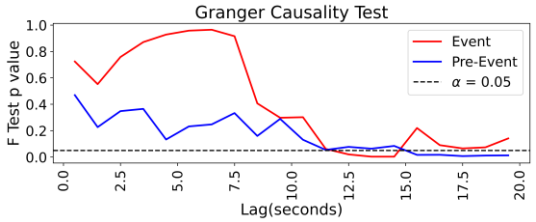

Figure 6. Granger Causality Results Q vs. V

Proof-of-Concept Simulation: Fig. 7 shows a PI type voltage controller with feedback delay to approximately recreate the inferred controller setup at the PV plant connected to Dominion's grid. The PV dynamics are assumed to be fast and stable and therefore represented by the algebraic equation $Q_r = Q$. Since the plant dynamics are extremely slow, response of the grid to them is modeled with the static load curve $V = a_0 + a_1 Q$. The gains of the PI controller gains are arbitrarily set to $k_p = 6$ and $k_i = 0.02$ with the voltage setpoint $V_r = 1.02$ pu. The data sampling rate is set to 2 Hz / $\Delta t = 0.5\,s$ with a measurement delay of 10 s (based on minimum inferred delay in the real system) or $n_d = \frac{10}{1/2} = 20$.

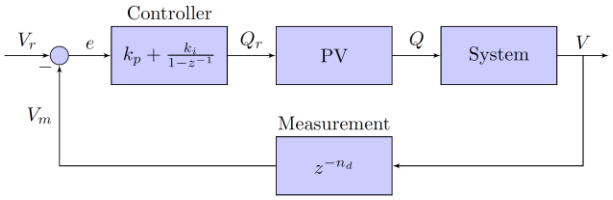

Figure 7. Control Diagram

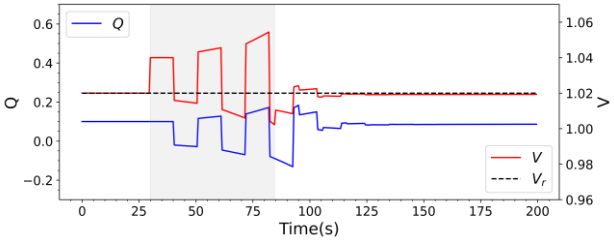

Figure 8. Simulated Square Wave Resulting from Large Delays

The event being simulated is a momentary change in the system operating curve parameters (a_0, a_1), to mimic a line tripping. The controller response is shown in Fig. 8 where the event period is shaded gray. During the event, the system becomes more sensitive to Q injection, resulting in a non-sinusoidal square-like response triggered by a jump in V at t = 30 s. This behavior starts to vanish when the event ends at t = 85 s, eventually converging to the equilibrium around t = 125 s. This shows how a change in the grid's operating conditions along with large delays in control loops can result in such atypical response, similar in nature to what was observed in the

real-world data in Fig. 2. Finally, we vary the measurement delay from 10-15 s and plot the spectral estimate from Q response of the controller for the same event in Fig. 9. In this case, the frequency of the dominant dynamics is equal to $\frac{1}{2\times(time\ delay)}$.

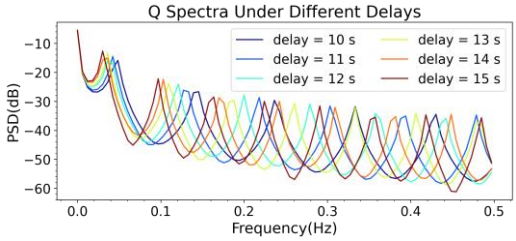

Figure 9 Effect of Delay on Dominant Frequency

IV. Conclusions

In this paper we present an atypical square wave-like characteristic response from a solar PV plant in the Dominion Energy service territory. Despite the lack of dynamic models, this work goes beyond traditional mode quantification by presenting a data-driven synchrophasor analysis to understand the root cause. Long feedback delays in the plant voltage controller were found to be the culprit, rather than the PV inverter controls themselves. Finally, the findings are demonstrated by a simulation of the mechanism.

V. References

[1] Y. Cheng *et al.*, "Real-World Subsynchronous Oscillation Events in Power Grids With High Penetrations of Inverter-Based Resources," *IEEE Trans. Power Syst.*, vol. 38, no. 1, pp. 316–330, Jan. 2023, doi: 10.1109/TPWRS.2022.3161418.

[2] C. Wang, C. Mishra, K. D. Jones, R. M. Gardner, and L. Vanfretti, "Identifying Oscillations Injected by Inverter-Based Solar Energy Sources," in *2022 IEEE Power & Energy Society General Meeting (PESGM)*, Jul. 2022, pp. 1–5. doi: 10.1109/PESGM48719.2022.9916830.

[3] L. Vanfretti, M. Baudette, J.-L. Domínguez-García, M. S. Almas, A. White, and J. O. Gjerde, "A Phasor Measurement Unit Based Fast Real-time Oscillation Detection Application for Monitoring Wind-farm-to-grid Sub–synchronous Dynamics," *Electr. Power Compon. Syst.*, vol. 44, no. 2, pp. 123–134, Jan. 2016, doi: 10.1080/15325008.2015.1101727.

[4] L. Vanfretti *et al.*, "Application of ambient analysis techniques for the estimation of electromechanical oscillations from measured PMU data in four different power systems," *Eur. Trans. Electr. Power*, vol. 21, no. 4, pp. 1640–1656, 2011, doi: 10.1002/etep.507.

[5] C. Mishra *et al.*, "Analysis of STATCOM Oscillations using Ambient Synchrophasor Data in Dominion Energy," in *2022 IEEE Power & Energy Society Innovative Smart Grid Technologies Conference (ISGT)*, Apr. 2022, pp. 1–5. doi: 10.1109/ISGT50606.2022.9817489.

[6] K. Gröchenig, *Foundations of Time-Frequency Analysis*. in Applied and Numerical Harmonic Analysis. Boston, MA: Birkhäuser, 2001. doi: 10.1007/978-1-4612-0003-1.

[7] J. Xu, H. Yang, and I. Daubechies, "Recursive Diffeomorphism-Based Regression for Shape Functions," *SIAM J. Math. Anal.*, vol. 50, no. 1, pp. 5–32, Jan. 2018, doi: 10.1137/16M1097535.

[8] "Inverter-Based Resource Performance Task Force." Accessed: Jun. 01, 2023. [Online]. Available: https://www.nerc.com/comm/PC/Pages/Inverter-Based-Resource-Performance-Task-Force.aspx

[9] L. Ljung, *System Identification: Theory for the User*, 2nd edition. Upper Saddle River, NJ: Pearson, 1998.

[10] C. W. J. Granger, "Investigating Causal Relations by Econometric Models and Cross-spectral Methods," *Econometrica*, vol. 37, no. 3, pp. 424–438, 1969, doi: 10.2307/1912791.